MANAS Journal of Engineering
ISSN 1694-7398 | e-ISSN 1694-7398

Volume11, Issue 2, (2023) Pages 204-215
https://doi.org/10.51354/mjen.1312700

Response surface methodology optimization of electrode modification parameters toward hydrazine electrooxidation on Pd/MWCNT/GCE

Berdan Ulas[1, 2, *]

[1] Department of Mining Engineering, Faculty of Engineering, Van Yuzuncu Yil University, Van, Turkey, berdanulas@yyu.edu.tr, ORCID: 0000-0003-0650-0316

[2] Department of Chemical Engineering, Institute of Natural and Applied Sciences, Van Yuzuncu Yil University, Van, Turkey,

ABSTRACT

In this study, MWCNT supported Pd (Pd/MWCNT) was synthesized by $NaBH_4$ reduction method as catalyst for hydrazine electrooxidation reaction (HEOR). Characterization methods namely inductively coupled plasma mass spectrometry (ICP-MS), elemental mapping, and scanning electron microscopy with energy dispersive X-ray (SEM-EDX) were used to analyze the surface morphology and metal composition of the catalysts. The Pd/MWCNT catalyst's average particle size is estimated to be 6.35 nm based on SEM images. Glassy carbon electrode (GCE) modification parameters namely the amount of catalyst ink transferred to the GCE surface (V_s), ultrasonication time of the catalyst ink (t_u), and the drying time of the Pd/MWCNT/GCE (t_d) were optimized by using response surface methodology as 4.92 µL, 1 min and 19.52 min, respectively. Experimental specific activity value for HEOR was obtained as 7.13 mA cm^{-2} with 2.59% deviation under optimum conditions. Optimization of electrode preparation conditions is an inexpensive and facile method that could be used to improve the performance of anode catalysts for fuel cells.

ARTICLE INFO

Research article

Received: 10.06.2023
Accepted: 26.06.2023

Keywords:
response surface methodology,
hydrazine,
electrocatalyst

*Corresponding author

1. Introduction

The increasing population, accelerating industrialization, and environmental pollution have been gradually increased the need for green energy [1]. Power conversion devices based on hydrogen energy are potential technologies to meet this energy demand. Fuel cells, especially proton exchange membrane fuel cells (PEMFCs), are promising power conversion systems due to their flexible operating temperature, environmental friendliness, and high energy density [2]. However, liquid fuel cells are preferred for their ease of transportation and storage, despite PEMFCs being the most popular type of fuel cells [3]. Fuels such as methanol [4], ethanol [5], formic acid [6], and $NaBH_4$ [7] have been frequently reported for direct liquid fuel cells. Among direct liquid fuel cells, direct methanol fuel cells (DMFCs) are the closest to commercialization [8, 9]. However, DMFCs have disadvantages such as greenhouse gas formation, high fuel crossover, and anode catalyst poisoning [9, 10]. Hydrazine has high potential as a fuel for fuel cells. Despite its high toxicity, hydrazine is easily accessible, does not contain carbon, and is cost-effective, making it a good alternative to other fuels [11]. The ability to store hydrazine as a solid (hydrazone) significantly reduces the risks associated with its high toxicity [12]. Direct hydrazine fuel cells (DHFCs) are environmentally friendly power conversion devices with only nitrogen and water as emissions [13, 14]. They can compete with DMFCs in terms of power density (5.4 kWh L^{-1}) and cell voltage (1.56 V) [15]. Unlike DMFCs, DHFCs do not suffer from CO poisoning in the anode catalyst since they do not contain carbon in their structure [13, 16]. The anode, cathode, and overall reactions in DHFCs are given in equation (1-3).

$$2N_2H_4 + 8OH^- \rightarrow N_2 + 4H_2O + 8e^- \quad (1)$$

$$O_2 + 2H_2O + 4e^- \rightarrow 4OH^- \quad (2)$$

$$2N_2H_4 + O_2 \rightarrow N_2 + 4H_2O \quad (3)$$

The electrooxidation of hydrazine is an important half-reaction for DHFCs due to its high conversion efficiency and rapid kinetics in an alkaline environment [17]. The hydrazine

electrooxidation reaction (HEOR) has a voltage-lowering effect compared to the oxygen evolution reaction [18]. Therefore, the design of anode catalysts with high activity, stability, and selectivity for HEOR is a critical issue for the commercialization of DHFCs. Catalyst systems composed of relatively inexpensive transition metals such as Cu [19], Ni [20], and Co [21] have been frequently reported to exhibit high performance in alkaline environments. However, the oxide layer formed on these catalysts negatively affects the activity and stability of the catalyst system for HEOR. Precious metals such as Rh, Ru, Pd, and Pt, despite their high cost, are widely preferred as DHFC anode catalysts due to their high performance for HEOR. Additionally, the performance of electrodes prepared with catalysts significantly affects the electrochemical efficiency. Optimization of electrode preparation parameters has been previously reported by our research group to significantly increase the specific activity of a conventional anode catalyst. Optimum electrode preparation parameters for glucose electrooxidation have been determined with Pd and Pt anode catalysts, and a 1.5-fold higher specific activity has been observed compared to similar catalysts in the literature [22].

In conventional optimization methods, such as one factor at a time, the effect of an independent variable on the response is examined at constant values of other parameters. The simultaneous analysis of the effects of parameters on the response brings statistical experimental design methods such as the response surface method to the fore. The response surface method establishes a mathematical model between the investigated parameters and the response function. It also enables numerical and graphical optimization with statistical analysis of the created mathematical model. RSM has been frequently reported by researchers for optimizing adsorption conditions [23]. Due to its advantages such as revealing the interaction of parameters, reduced number of experiments and chemical amount, RSM has started to be used in other fields as well.

In this study, the Pd/MWCNT catalyst was prepared via $NaBH_4$ reduction method and characterized using scanning electron microscopy with energy dispersive X-ray spectroscopy (SEM/EDX), elemental mapping, and inductively coupled plasma mass spectrometry (ICP-MS). The glassy carbon electrode (GCE) modified with Pd/MWCNT was investigated for anode catalyst performance for HEOR, and the optimum electrode preparation conditions were determined using RSM. The optimization of electrode preparation parameters for Pd/MWCNT/GCE toward HEOR has not been reported in the literature yet. By optimizing the electrode preparation parameters of Pd/MWCNT/GCE, electrodes with lower cost and higher specific activity were obtained.

2. Materials and methods

2.1. Synthesis and characterization of Pd/MWCNT

The typical $NaBH_4$ reduction method was used to synthesis of MWCNT supported Pd [24]. First, 10 ml of distilled water were used to dissolve the analytical grade K_2PdCl_4 that was employed as a precursor. The specified amount of MWCNT was added to the solution. The $NaBH_4$ solution was then added dropwise and the mixture agitated on a magnetic stirrer for the following 2 h. After the reduction was finished, the final solution was agitated for 24 h before being filtered, washed, and dried at 80°C. SEM-EDX, elemental mapping, and ICP-MS were utilized as analytical techniques for characterization of the Pd/MWCNT. The elemental composition and morphological features of Pd/MWCNT were investigated through SEM-EDX with elemental mapping (Zeiss Sigma 300) and ICP-MS (Agilent 7800).

2.2. Electrochemical evaluation

Electrochemical experiments were performed using a CH Instrument 660E Potentiostat/Galvanostat with conventional three electrodes. A catalyst slurry was formed by dissolving 3 mg of MWCNT in 1 ml of Nafion in an ultrasonic water bath for 10 minutes in order to modify the working electrode. The glassy carbon electrode (GCE) was sprayed with the prepared catalyst slurry, and it was then dried for the identified lengths of time (t_d) at room temperature.

2.3. Response surface methodology

The GCE electrode was modified with Pd/MWCNT and the modification conditions were optimized with the RSM center composite design (CCD). The amount of catalyst ink transferred to the GCE surface, the ultrasonication time of the catalyst ink, and the drying time of the Pd/MWCNT/GCE electrode were chosen as independent variables for the modification of GCE, and are indicated by A (V_s), B (t_u), and C (t_d), respectively. The A, B, and C parameter ranges for HEOR on Pd/MWCNT/GCE and the specific activity values at the determined experimental points are presented in Table 1. The -1, 0, and +1 shown in Table 1 represent the minimum, middle, and maximum points, respectively. The experimental program proposed by Design Expert consists of 6 replicate points and 14 different points.

.

Table 2. *CCD for HEOR on Pd/MWCNT/GCE.*

Run	Factor 1 A:V_s (µL)	Factor 2 B:t_u (min)	Factor 3 C:t_d (min)	Response Specific Activity for HEOR (mA cm^{-2})
1	10 (+1)	60 (+1)	40 (+1)	39.92
2	10 (+1)	1 (-1)	1 (-1)	5.23
3	0.5 (-1)	60 (+1)	1 (-1)	7.32
4	5.25 (0)	30.5 (0)	20.5 (0)	5.12
5	0.5 (-1)	60 (+1)	40 (+1)	6.21
6	5.25 (0)	60 (+1)	20.5 (0)	20.65
7	10 (+1)	1 (-1)	40 (+1)	11.40
8	10 (+1)	30.5 (0)	20.5 (0)	4.18
9	10 (+1)	60 (+1)	1 (-1)	9.33
10	5.25 (0)	30.5 (0)	20.5 (0)	4.83
11	5.25 (0)	30.5 (0)	1 (-1)	1.61
12	5.25 (0)	30.5 (0)	20.5 (0)	5.30
13	5.25 (0)	30.5 (0)	20.5 (0)	5.18
14	5.25 (0)	30.5 (0)	40 (+1)	3.79
15	0.5 (-1)	1 (-1)	1 (-1)	9.05
16	5.25 (0)	30.5 (0)	20.5 (0)	4.55
17	5.25 (0)	30.5 (0)	20.5 (0)	3.97
18	5.25 (0)	1 (-1)	20.5 (0)	1.23
19	0.5 (-1)	30.5 (0)	20.5 (0)	1.09
20	0.5 (-1)	1 (-1)	40 (+1)	5.27

3. Results and discussion

3.1. Physical characterization

The surface morphology of Pd/MWCNT was examined by SEM and is shown in Figure 1. From Figure 1a and b the network of the CNT is clearly visible. It was determined from Figure 1c and d that Pd did not agglomerate on the CNT surface. It was also observed that Pd nanoparticles adhered to both the inner and outer walls of the CNT (Figure 1e and f). The mean particle size of Pd nanoparticles in SEM images was determined as 6.35 nm with ImageJ software. Elemental mapping analysis to Pd/MWCNT was performed to confirm the distribution of Pd nanoparticles. C, O, Pd, and overlay elemental mapping images of Pd/MWCNT are shown in Figure 2. Since the metal ratio of Pd/MWCNT to the support material is 10% by weight, it is clearly seen that carbon is more dominant than other elements in the elemental mapping images (Figure 2a). Furthermore, the oxygen detected in the catalyst structure was attributed to the presence of PdO, since K_2PdCl_4 cannot be fully reduced with $NaBH_4$ and Pd is easily oxidized (Figure 2b) [25]. It was observed from Figure 2c that the Pd nanoparticles were homogeneously dispersed on the MWCNT. Also from the overlay images of all elements, it is more clearly seen as the elements are uniformly distributed on MWCNT (Figure 2d). Pd, O and C peaks were detected in the EDX spectrum of Pd/MWCNT. Carbon exhibited a very high peak intensity, while the intensity of the oxygen peak was very weak. In this context, the EDX spectrum also support the elemental mapping results. ICP-MS results of Pd/MWCNT were determined as 11.2:100 of Pd:MWCNT by mass. The closeness of the obtained metal ratio to the targeted ratio indicates that the synthesis was successful.

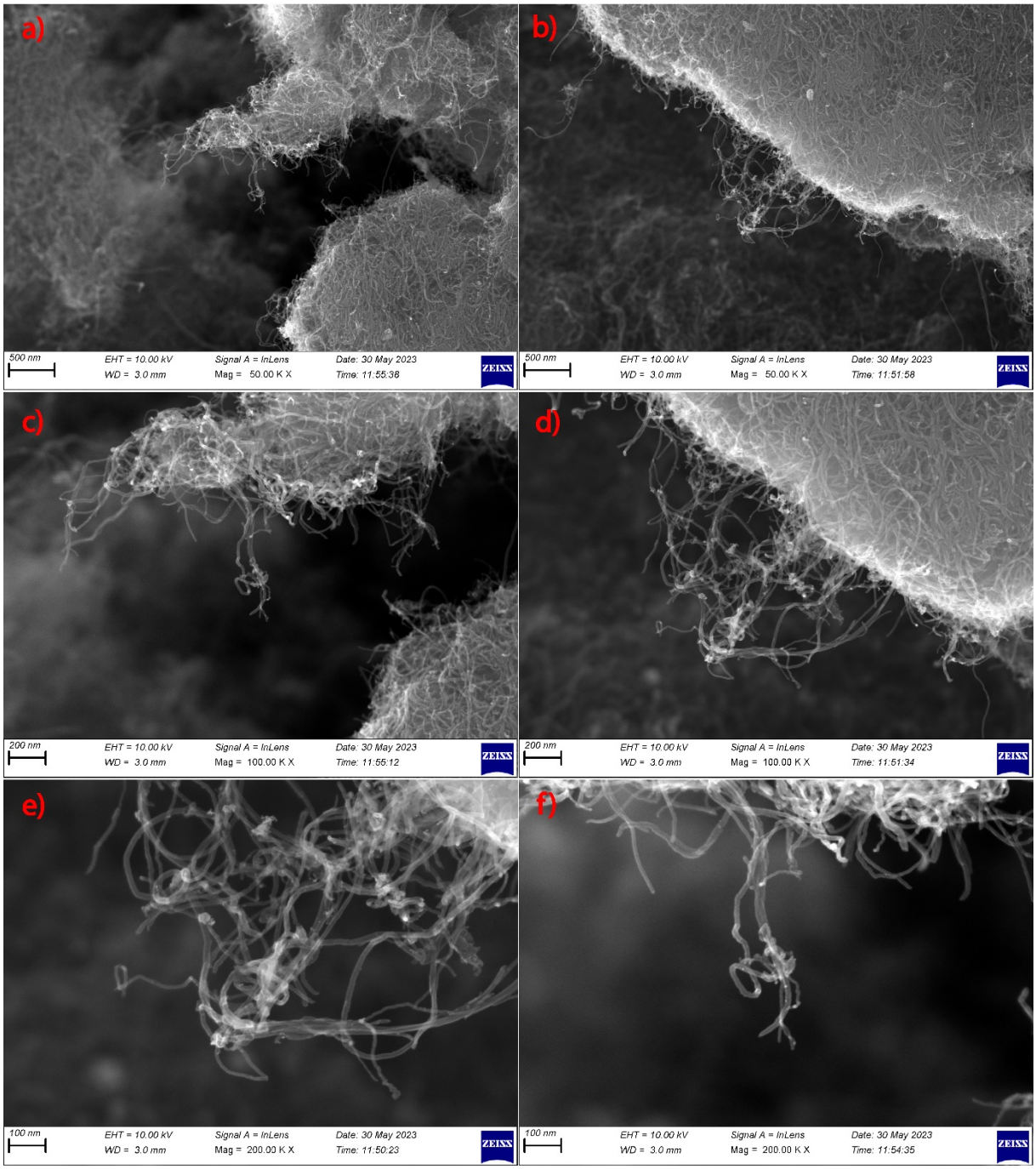

Figure 1. *SEM images of Pd/MWCNT.*

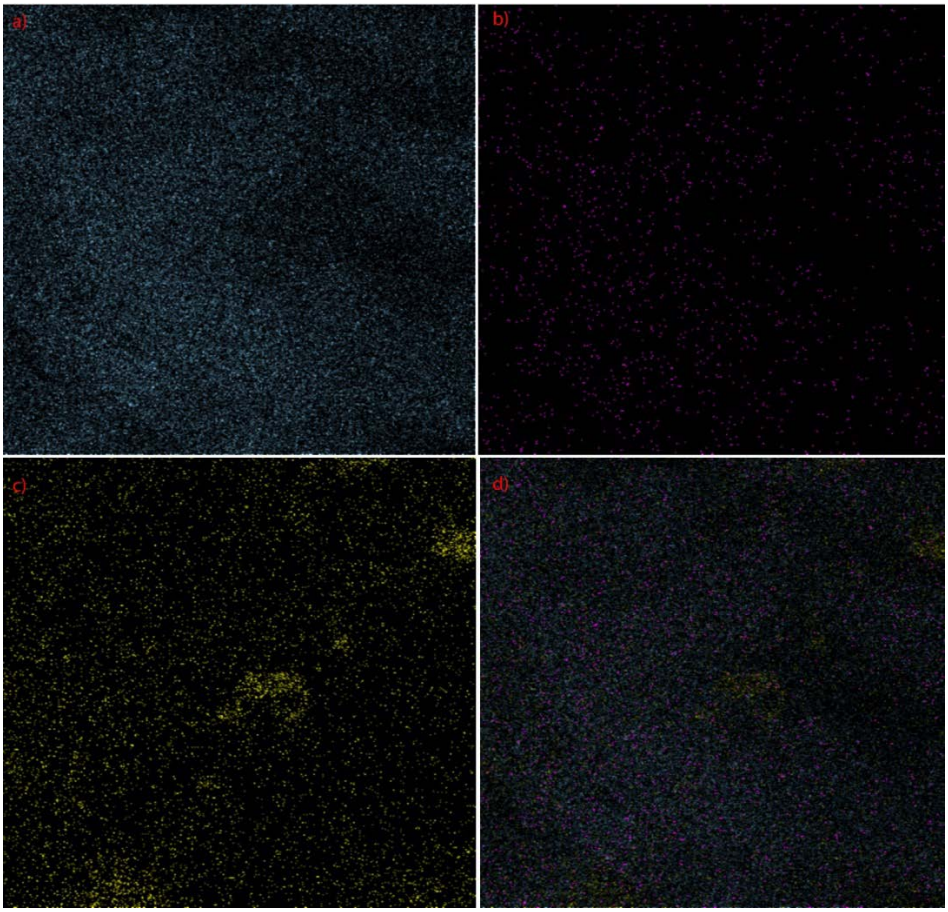

Figure 2. *SEM images of Pd/MWCNT.*

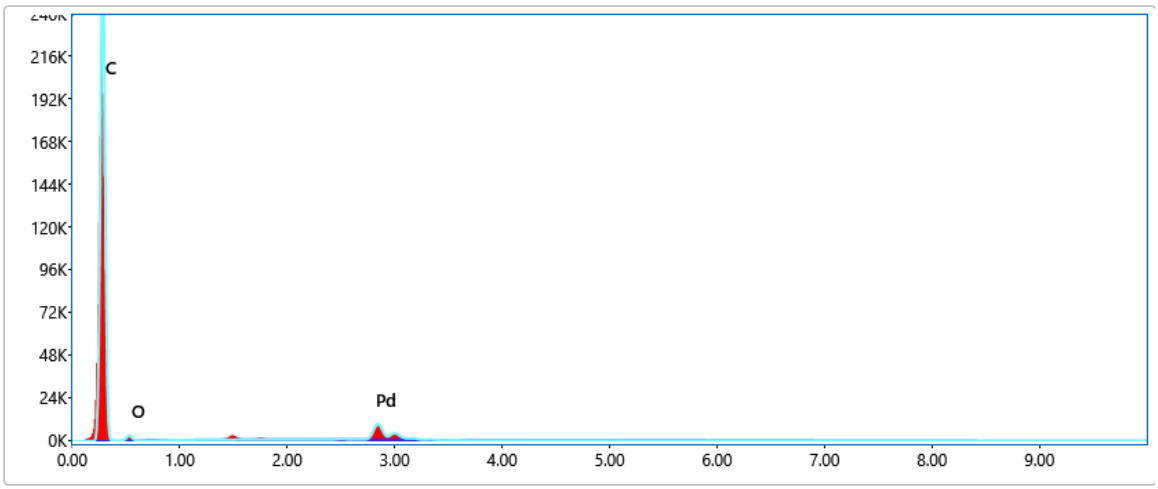

Figure 3. *EDX spectrum for Pd/MWCNT.*

3.2. Response surface methodology

The specific activities for HEOR of the Pd/MWCNT/GCE electrode prepared at the V_s, t_u and t_d values given in Table 1 were determined in 0.1 M KOH + 0.02 M N_2H_2 solutions. Voltammograms of each experimental set are given in Figure 4. The

obtained results were statistically analyzed with the Design Expert software.

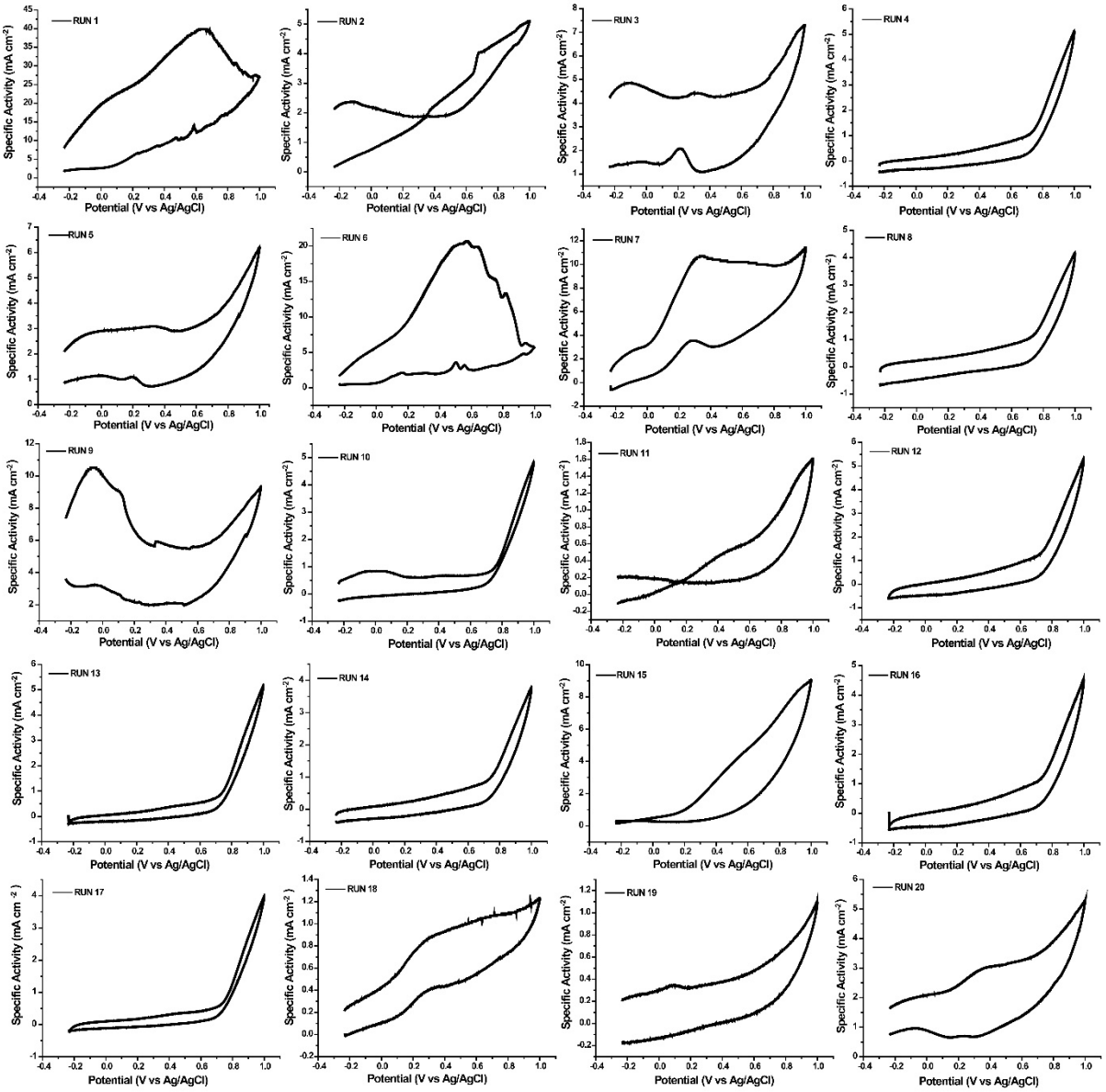

Figure 4. *CV profiles for CCD.*

The model with which the experimental results were compatible was investigated with the Design Expert software and is given in Tables 2 and 3. Table 2 exhibites that the lack of fit tests of linear, 2FI and quadratic models suggested by the software are statistically significant, while the cubic model is aliased. In this case, it is understood that cubic model terms cannot be estimated individually and the cubic model should be used as a summary of these combined effects. According to the lack fit test results, except for the aliased cubic model, the lowest F value is the quadratic model with 124.72. As can be seen from Table 3, the R^2 values of the cubic, quadratic, 2FI and linear models were obtained as 0.991, 0.893, 0692 and 0.38, respectively. Because of the aliased model terms it contains, the highest correlation coefficient is reported for the cubic model. In addition, the quadratic model showed the lowest standard deviation and PRESS values (excluding linear model) with 3.927 and 2072.65, respectively. When the statistical parameters reported for the models suggested by the software are evaluated together, it is concluded that the model with the highest predictive performance is the quadratic model.

Table 2. *Lack of fit tests for suggested models.*

Source	Sum of Squares	df	Mean Square	F Value	p-value Prob > F	
Linear	891.17	11	81.01	330.18	< 0.0001	
2FI	442.73	8	55.34	225.54	< 0.0001	
Quadratic	153.01	5	30.60	124.72	< 0.0001	Suggested
Cubic	11.308	1	11.31	46.087	0.0011	Aliased
Pure Error	1.2268	5	0.245			

Table 3. *Model summary statistics for HEOR on Pd/MWCNT/GCE.*

Source	Std. Dev.	R-Squared	Adjusted R-Squared	PRESS	
Linear	7.468	0.38	0.264	1858.68	
2FI	5.844	0.692	0.549	2978.18	
Quadratic	3.927	0.893	0.796	2072.65	Suggested
Cubic	1.445	0.991	0.972	13896.1	Aliased

The proposed quadratic model in terms of actual values and coded for HEOR on Pd/MWCNT/GCE is shown in Eqn. (3-4). Analysis of variance (ANOVA) was performed for the proposed model and is given in Table 4. It is known that a p value less than 0.05 in the 95% confidence interval indicates that the relevant model term is statistically significant. Accordingly, it is seen that the suggested model terms A, B, C, AB, AC, BC and B^2 are statistically significant. A^2 and C^2 terms were not statistically significant with p values of 0.8897 and 0.9106. However, the terms A^2 and C^2 were not removed from the model, as it was concluded that the model improved the predictive performance [23].

Specific Activity for HEOR =

$$+4.08+4.11*A+5.12*B+3.41*C+4.18*A*B+5.21*A*C+3.39*B*C-0.34*A^2+7.97*B^2-0.27*C^2 \quad (3)$$

Specific activity for HEOR =

$$+12.97337-(1.03953*V_s)-(0.66207*t_u)-(0.27075*t_d)+(0.029819*V_s*t_u)+(0.056216*V_s*t_d)+(5.89115E-003*t_u*t_d)-(0.014935*V_s2)+(0.00915484*t_u2)-(0.000717167*t_d2) \quad (4)$$

Table 4. *ANOVA table for HEOR on Pd/MWCNT/GCE.*

Source	**Sum of Squares**	**df**	**Mean Square**	**F Value**	**p-value Prob > F**	
Model	1285.75	9	142.86	9.26	0.0009	significant
A-V_s	169.03	1	169.03	10.96	0.0079	
B- t_u	262.56	1	262.56	17.02	0.0021	
C- t_d	115.99	1	115.99	7.52	0.0207	
AB	139.67	1	139.67	9.06	0.0131	
AC	216.9	1	216.9	14.06	0.0038	
BC	91.88	1	91.88	5.96	0.0348	
A^2	0.31	1	0.31	0.02	0.8897	
B^2	174.55	1	174.55	11.32	0.0072	
C^2	0.2	1	0.2	0.013	0.9106	
Residual	154.24	10	15.42			

Pure Error	1.23	5	0.25
Cor Total	1439.99	19	

In Figure 5, the compatibility of the quadratic model and experimental data is discussed. The distribution of model data relative to the actual data for HEOR on Pd/MWCNT is shown in Figure 5. Although very few of the experimental points expected to be dispersed around the diagonal deviated, it was observed that the majority of them dispersed around the diagonal. Figure 5b shows the distribution of errors. It has been determined that the errors are distributed around the standard line. The random distribution of errors indicates that there is no systematic error. The plot of the residuals against the predicted values is given in Figure 5c. The random distribution between the boundary lines determined by the software is explained by the non-constant variance. The plot of the residues according to the experiment number is exhibited in Figure 5d. It has been determined that the graph obtained as a result of combining the residual values with a line does not show a recurrent trend. Therefore, it was concluded that the residuals were not caused by a systematic error. Model validation graphs and ANOVA test results show that the proposed quadratic model is a good predictor.

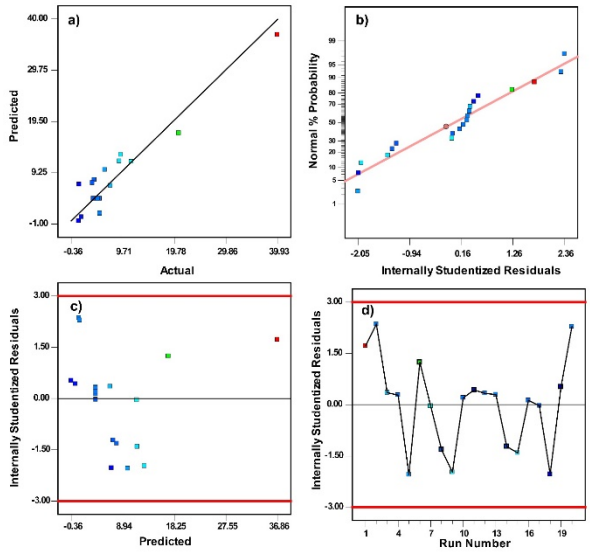

Figure 4. *Model validation plots for HEOR on Pd/MWCNT/GCE.*

In Figure 6, response surface plots of V_s, t_u and t_d are presented. The binary interactions of t_u and V_s are shown in Figure 6a. When the t_u value was increased from 1 min to 30.5 min, a decrease of 1.627 mA cm^{-2} in the specific activity was observed (V_s=5.25 µL and t_d=20.5 min). After the t_u value of 30.5 min, the specific activity increased sharply and reached 17.175 mA cm^{-2} (Figure 6a). At constant t_u=30.5 min and t_d=20.5 min, when V_s was increased from 0.5 µL to 5.25 µL, the specific activity for HEOR increased from 1.097 mA cm^{-2} to 4.828 mA cm^{-2} (Figure 6b). After the V^s value of 5.25 µL, the specific activity gradually decreased to a value of 4.175 mA cm^{-2}. From Figure 6c, as a result of increasing t_d from 1 min to 40 min, the specific activity increased almost linearly from 0.405 mA cm^{-2} to 7.217 mA cm^{-2}.

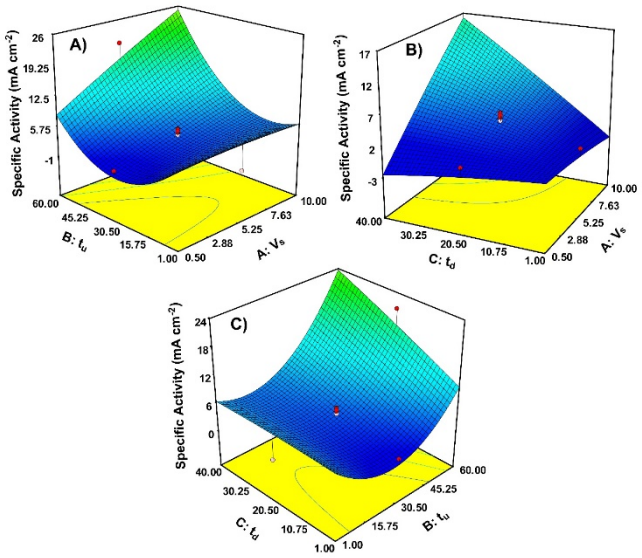

Figure 6. *Response surface plots for HEOR on Pd/MWCNT/GCE A) t_u vs V_s, B) t_d vs V_s, and C)t_d vs t_u.*

Numerical optimization was performed for HEOR on Pd/MWCNT/GCE with Design Expert software. In the optimization process, the specific activity value is maximized by minimizing V_s, t_u and t_d. While the optimum V_s, t_u and t_d values were determined as 4.92 µL, 1 min and 19.52 min, respectively, the model specific activity value was found as 6.95 mA cm^{-2}. Experimental specific activity value for HEOR was determined as 7.13 mA cm^{-2} with 2.59% deviation by CV measurements performed under optimum conditions.

The electrochemical behavior of Pd/MWCNT at optimum conditions determined by RSM is given in Figure 7. Electrochemical experiments were carried out at a scanning rate of 100 mV s^{-1} and in 0.1 M KOH+0.02 M N_2H_2 solution. Figure 7a exhibits the voltammogram of Pd/MWCNT in a 0.1 M KOH support electrolyte. In the forward scan, no electrochemical phenomena were observed between 0 V and 0.3 V, and it was concluded that this potential range is a double layer region [26]. The narrow peak observed at a potential of about 0.3 V in reverse scan is due to PdO reduction [27]. 50 cycle CV profiles of Pd/MWCNT are given in Figure 7b. Pd/MWCNT showed 7.13 mA cm^{-2} specific activity under optimum electrode preparation conditions and this specific activity decreased to 1.42 mA cm^{-2} after 50

cycles. The decrease in the activity of Pd/MWCNT could be attributed to the accumulation of intermediate compound on the electrode surface [28].

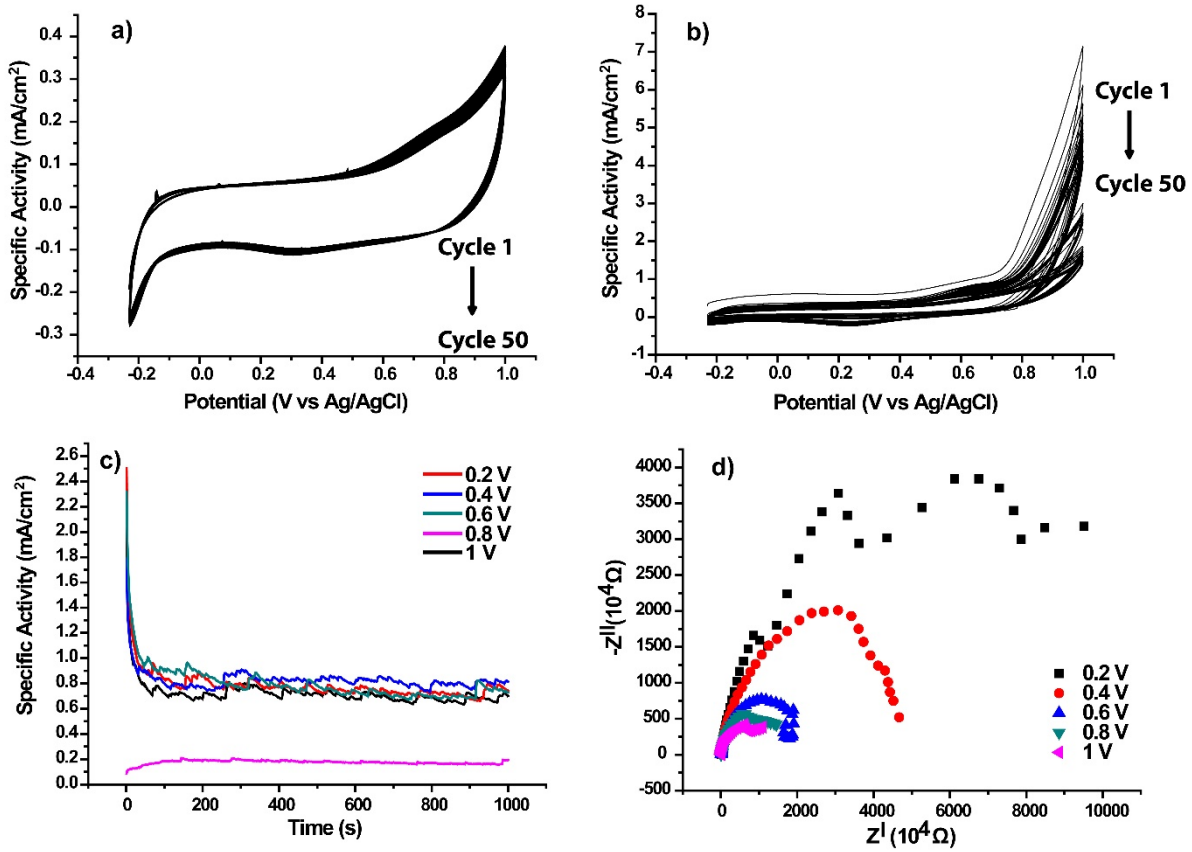

Figure 7. *a) CV in 0.1 M KOH, b) CV in 0.1 M KOH + 0.02 M N_2H_2, c) CA curves at 0.2-1 V in 0.1 M KOH + 0.02 M N_2H_2, and d) EIS profiles at 0.2-1 V in 0.1 M KOH + 0.02 M N_2H_2.*

Chronoamperometric curves of Pd/MWCNT at 0.2, 0.4, 0.6, 0.8, and 1 V potentials are presented in Figure 7c. Except for the CA curve at 0.8 V potential, all CA profiles are similar to each other. Pd/MWCNT exhibited good stability over 1000 s despite fluctuations in current. EIS curves of Pd/MWCNT at varying potentials are given in Figure 7d. It is known that as the diameter of the EIS curves decreases, the charge transfer resistance decreases and the electrocatalytic activity increases [29]. In this direction, as can be seen from Figure 7d, the electrocatalytic activity of Pd/MWCNT increased as the applied potential increased. In this case, it was concluded that the HEOR mechanism on Pd/MWCNT/GCE is predominantly driven by charge transfer kinetics.

4. Conclusion

In this study, GCE was modified with Pd/MWCNT catalysts synthesized by the $NaBH_4$ reduction method and its performance as a catalyst for HEOR was investigated. From the SEM-EDX results, it was determined that the average particle size of Pd/MWCNT was 6.35 nm. Elemental mapping results show that Pd is homogeneously distributed on MWCNT, and the metal composition of Pd/MWCNT was determined as 11.2% by ICP-MS. Optimum electrode preparation conditions for HEOR on Pd/MWCNT/GCE were determined by RSM as 4.92 µL V_s, 1 min t_u, and 19.52 min t_d. Under optimum conditions, experimental specific activity value for HEOR was obtained as 7.13 mA cm^{-2} with 2.59% deviation. The R^2 value of the proposed quadratic model for HEOR on Pd/MWCNT/GCE was determined as 0.893, and the model was found to be statistically significant in according to the ANOVA test. This study clearly revealed that the use of optimization methods for the electrode preparation stage is very important in terms of increasing the specific activity. It is concluded that conducting electrode optimization researches for future designed catalysts will bring cheaper, stable and active catalysts to the literature.

References

[1]. Su, M., Wang, Q., Li, R., Wang, L. "Per Capita Renewable Energy Consumption in 116 Countries: The Effects of Urbanization, Industrialization, Gdp, Aging, and Trade Openness", Energy, 254, (2022), 124289; Li, W., Yu, X., Hu, N., Huang, F., Wang, J., Peng, Q. "Study on the Relationship between Fossil Energy Consumption and Carbon Emission in Sichuan Province", Energy Reports, 8, (2022), 53-62.

[2]. Nguyen, H. Q., Shabani, B. "Proton Exchange Membrane Fuel Cells Heat Recovery Opportunities for Combined Heating/Cooling and Power Applications", Energy Conversion Management, 204, (2020), 112328; Jamil, A., Rafiq, S., Iqbal, T., Khan, H. A. A., Khan, H. M., Azeem, B., Mustafa, M., Hanbazazah, A. S. "Current Status and Future Perspectives of Proton Exchange Membranes for Hydrogen Fuel Cells", Chemosphere, (2022), 135204; Yeetsorn, R., Maiket, Y., Kaewmanee, W. "The Observation of Supercapacitor Effects on Pemfc–Supercapacitor Hybridization Performance through Voltage Degradation and Electrochemical Processes", RSC advances, 10, (2020), 13100-13111.

[3]. Wan, Z., Tao, Y., Shao, J., Zhang, Y., You, H. "Ammonia as an Effective Hydrogen Carrier and a Clean Fuel for Solid Oxide Fuel Cells", Energy Conversion Management, 228, (2021), 113729; Li, M., Bai, Y., Zhang, C., Song, Y., Jiang, S., Grouset, D., Zhang, M. "Review on the Research of Hydrogen Storage System Fast Refueling in Fuel Cell Vehicle", International Journal of Hydrogen Energy, 44, (2019), 10677-10693.

[4]. Ulas, B., Caglar, A., Kivrak, A., Kivrak, H. "Atomic Molar Ratio Optimization of Carbon Nanotube Supported Pdauco Catalysts for Ethylene Glycol and Methanol Electrooxidation in Alkaline Media", Chemical Papers, 73, (2019), 425-434; Zhao, F., Zheng, L., Yuan, Q., Yang, X., Zhang, Q., Xu, H., Guo, Y., Yang, S., Zhou, Z., Gu, L. "Ultrathin Pdaubite Nanosheets as High-Performance Oxygen Reduction Catalysts for a Direct Methanol Fuel Cell Device", Advanced Materials, 33, (2021), 2103383.

[5]. Zheng, Y., Wan, X., Cheng, X., Cheng, K., Dai, Z., Liu, Z. "Advanced Catalytic Materials for Ethanol Oxidation in Direct Ethanol Fuel Cells", Catalysts, 10, (2020), 166; Wang, K., Wang, F., Zhao, Y., Zhang, W. "Surface-Tailored Ptpdcu Ultrathin Nanowires as Advanced Electrocatalysts for Ethanol Oxidation and Oxygen Reduction Reaction in Direct Ethanol Fuel Cell", Journal of Energy Chemistry, 52, (2021), 251-261.

[6]. Caglar, A., Ulas, B., Cogenli, M. S., Yurtcan, A. B., Kivrak, H. "Synthesis and Characterization of Co, Zn, Mn, V Modified Pd Formic Acid Fuel Cell Anode Catalysts", Journal of Electroanalytical Chemistry, 850, (2019), 113402; Ulas, B., Kivrak, A., Aktas, N., Kivrak, H. "Carbon Monoxide and Formic Acid Electrooxidation Study on Au Decorated Pd Catalysts Prepared Via Microwave Assisted Polyol Method", Fullerenes, Nanotubes Carbon Nanostructures, 27, (2019), 545-552.

[7]. Kaya, S., Yilmaz, Y., Er, O. F., Alpaslan, D., Ulas, B., Dudu, T. E., Kivrak, H. "Highly Active Rupd Bimetallic Catalysts for Sodium Borohydride Electrooxidation and Hydrolysis", Journal of Electronic Materials, 51, (2022), 403-411; Ulas, B., Alpaslan, D., Yilmaz, Y., Dudu, T. E., Er, O. F., Kivrak, H. "Disentangling the Enhanced Catalytic Activity on Ga Modified Ru Surfaces for Sodium Borohydride Electrooxidation", Surfaces Interfaces, 23, (2021), 100999.

[8]. Martinaiou, I., Videla, A. H. M., Weidler, N., Kübler, M., Wallace, W. D. Z., Paul, S., Wagner, S., Shahraei, A., Stark, R. W., Specchia, S. "Activity and Degradation Study of an Fe-Nc Catalyst for Orr in Direct Methanol Fuel Cell (Dmfc)", Applied Catalysis B: Environmental, 262, (2020), 118217; Ulas, B., Yagizatli, Y., Demir-Kivrak, H. (2022) Metal-Free Catalysts for Fuel Cell Applications, In *Carbon-Based Metal Free Catalysts*, pp 67-109, Elsevier.

[9]. Osman, S. H., Kamarudin, S. K., Basri, S., A. Karim, N. "Three-Dimensional Graphene Aerogel Supported on Efficient Anode Electrocatalyst for Methanol Electrooxidation in Acid Media", Catalysts, 13, (2023), 879.

[10]. Fadzillah, D., Kamarudin, S., Zainoodin, M., Masdar, M. "Critical Challenges in the System Development of Direct Alcohol Fuel Cells as Portable Power Supplies: An Overview", International Journal of Hydrogen Energy, 44, (2019), 3031-3054; Zakaria, Z., Kamarudin, S. K., Abd Wahid, K. A., Hassan, S. H. A. "The Progress of Fuel Cell for Malaysian Residential Consumption: Energy Status and Prospects to Introduction as a Renewable Power Generation System", Renewable Sustainable Energy Reviews, 144, (2021), 110984.

[11]. Zhang, Z., Tang, P., Wen, H., Wang, P. "Bicontinuous Nanoporous Ni-Fe Alloy as a Highly Active Catalyst for Hydrazine Electrooxidation", Journal of Alloys Compounds, 906, (2022), 164370; Askari, M. B., Salarizadeh, P., Beitollahi, H., Tajik, S., Eshghi, A., Azizi, S. "Electro-Oxidation of Hydrazine on Nife2o4-Rgo as a High-Performance Nano-Electrocatalyst in Alkaline Media", Materials Chemistry Physics, 275, (2022), 125313.

[12]. Luo, L., Cheng, J., Chen, S., Zhang, P., Chen, S., Tang, Z., Zeng, R., Xu, M., Hao, Y. "A near-Infrared Ratiometric Fluorescent Probe for Hydrazine and Its Application for Gaseous Sensing and Cell Imaging", Spectrochimica Acta Part A: Molecular Biomolecular Spectroscopy, 296, (2023), 122692.

[13]. Hosseini, M. G., Abdolmaleki, M., Daneshvari-Esfahlan, V. "Fabrication and Evaluation of the Performance of Co/Coniznag Nanoporous Structures as a Good Candidate for Using as Anode Catalyst in a Hydrazine Fuel Cell", Materials Technology, 34, (2019), 697-703.

[14]. Liu, W., Xie, J., Guo, Y., Lou, S., Gao, L., Tang, B. "Sulfurization-Induced Edge Amorphization in Copper–Nickel–Cobalt Layered Double Hydroxide Nanosheets Promoting Hydrazine Electro-Oxidation", Journal of Materials Chemistry A, 7, (2019), 24437-24444.

[15]. Feng, Z., Li, D., Wang, L., Sun, Q., Lu, P., Xing, P., An, M. "In Situ Grown Nanosheet Nizn Alloy on Ni Foam for High Performance Hydrazine Electrooxidation", Electrochimica Acta, 304, (2019), 275-281; Hwang, H., Hong, S., Kim, D.-H., Kang, M.-S., Park, J.-S., Uhm, S., Lee, J. "Optimistic Performance of Carbon-Free Hydrazine Fuel Cells Based on Controlled Electrode Structure and Water Management", Journal of Energy Chemistry, 51, (2020), 175-181.

[16]. Balčiūnaitė, A., Budrytė, E., Vaičiūnienė, J., Niaura, G., Kruusenberg, I., Kaare, K., Volperts, A., Dobele, G., Zurins, A., Tamašauskaitė-Tamašiūnaitė, L. "One-Pot Synthesis of Nitrogen-Doped Carbon Supported Mn-Co Nanoparticles for Hydrazine Oxidation", ECS Transactions, 97, (2020), 593.

[17]. Feng, Z., Zhang, H., Gao, B., Lu, P., Li, D., Xing, P. "Ni–Zn Nanosheet Anchored on Rgo as Bifunctional Electrocatalyst for Efficient Alkaline Water-to-Hydrogen Conversion Via Hydrazine Electrolysis", International Journal of Hydrogen Energy, 45, (2020), 19335-19343; Wang, T., Cao, X., Jiao, L. "Progress in Hydrogen Production Coupled with Electrochemical Oxidation of Small Molecules", Angewandte Chemie International Edition, (2022), e202213328.

[18]. Liu, X., Han, Y., Guo, Y., Zhao, X., Pan, D., Li, K., Wen, Z. "Electrochemical Hydrogen Generation by Oxygen Evolution Reaction-Alternative Anodic Oxidation Reactions", Advanced Energy Sustainability Research, 3, (2022), 2200005.

[19]. Crisafulli, R., de Paula, D. F., Zignani, S. C., Spadaro, L., Palella, A., Boninelli, S., Dias, J. A., Linares, J. J. "Promoting Effect of Cu on Pd Applied to the Hydrazine Electro-Oxidation and Direct Hydrazine Fuel Cells", Catalysts, 12, (2022), 1639; Wang, W., Wang, Y., Liu, S., Yahia, M., Dong, Y., Lei, Z. "Carbon-Supported Phosphatized Cuni Nanoparticle Catalysts for Hydrazine Electrooxidation", International Journal of Hydrogen Energy, 44, (2019), 10637-10645; Jiang, H., Wang, Z., Kannan, P., Wang, H., Wang, R., Subramanian, P., Ji, S. "Grain Boundaries of Co (Oh) 2-Ni-Cu Nanosheets on the Cotton Fabric Substrate for Stable and Efficient Electro-Oxidation of Hydrazine", International Journal of Hydrogen Energy, 44, (2019), 24591-24603.

[20]. Feng, Z., Li, D., Wang, L., Sun, Q., Lu, P., Xing, P., An, M. J. E. A. "In Situ Grown Nanosheet Nizn Alloy on Ni Foam for High Performance Hydrazine Electrooxidation", 304, (2019), 275-281; Chen, C., Wen, H., Tang, P.-P., Wang, P. "Supported Ni@ Ni2p Core–Shell Nanotube Arrays on Ni Foam for Hydrazine Electrooxidation", ACS Sustainable Chemistry Engineering, 9, (2021), 4564-4570; Wen, H., Gan, L.-Y., Dai, H.-B., Wen, X.-P., Wu, L.-S., Wu, H., Wang, P. "In Situ Grown Ni Phosphide Nanowire Array on Ni Foam as a High-Performance Catalyst for Hydrazine Electrooxidation", Applied Catalysis B: Environmental, 241, (2019), 292-298.

[21]. Li, J., Dong, C., Guo, M., Gao, W., Kang, L., Lei, F., Hao, P., Xie, J., Tang, B. "Cerium-Induced Lattice Disordering in Co-Based Nanocatalysts Promoting the Hydrazine Electro-Oxidation Behavior", Chemical Communications, 58, (2022), 6845-6848; Feng, G., An, L., Li, B., Zuo, Y., Song, J., Ning, F., Jiang, N., Cheng, X., Zhang, Y., Xia, D. "Atomically Ordered Non-Precious Co3ta Intermetallic Nanoparticles as High-Performance Catalysts for Hydrazine Electrooxidation", Nature Communications, 10, (2019), 4514; Firdous, N., Janjua, N. K. "Coptx/Γ-Al2o3 Bimetallic Nanoalloys as Promising Catalysts for Hydrazine Electrooxidation", Heliyon, 5, (2019), e01380.

[22]. Kaya, S., Ulas, B., Duzenli, D., Onal, I., Er, O. F., Yilmaz, Y., Tezsevin, I., Kivrak, H. "Glucose Electrooxidation Modelling Studies on Carbon Nanotube Supported Pd Catalyst with Response Surface Methodology and Density Functional Theory", Journal of Physics and Chemistry of Solids, 168, (2022), 110810; Kaya, S., Ulas, B., Er, O. F., Yılmaz, Y., Kivrak, H. "Optimization of Electrode Preperation Conditions for Enhanced Glucose Electrooxidation on Pt/Cnt by Response Surface Methodology", Journal of Electronic Materials, 51, (2022), 2971-2981.

[23]. Yılmaz, Ş. "Facile Synthesis of Surfactant-Modified Layered Double Hydroxide Magnetic Hybrid Composite and Its Application for Bisphenol a Adsorption: Statistical Optimization of Operational Variables", Surfaces and Interfaces, 32, (2022), 102171.

[24]. Ulas, B., Caglar, A., Sahin, O., Kivrak, H. "Composition Dependent Activity of Pdagni Alloy Catalysts for Formic Acid Electrooxidation", Journal of Colloid and Interface Science, 532, (2018), 47-57.

[25]. Cao, Z., Chen, H., Zhu, S., Zhang, W., Wu, X., Shan, G., Ziener, U., Qi, D. "Preparation of Janus Pd/Sio2 Nanocomposite Particles in Inverse Miniemulsions", Langmuir, 31, (2015), 4341-4350.

[26]. Lima, C. C., Rodrigues, M. V., Neto, A. F., Zanata, C. R., Pires, C. T., Costa, L. S., Solla-Gullon, J., Fernandez, P. S. "Highly Active Ag/C Nanoparticles Containing Ultra-Low Quantities of Sub-Surface Pt for the Electrooxidation of Glycerol in Alkaline Media", Applied Catalysis B: Environmental, 279, (2020), 119369; Kopač Lautar, A., Bitenc, J., Rejec, T., Dominko, R., Filhol, J.-S., Doublet, M.-L. "Electrolyte Reactivity in the Double Layer in Mg Batteries: An Interface Potential-Dependent Dft Study", Journal of the American Chemical Society, 142, (2020), 5146-5153.

[27]. Qiu, C., Wang, S., Gao, R., Qin, J., Li, W., Wang, X., Zhai, Z., Tian, D., Song, Y. "Low-Temperature Synthesis of Pdo-Ceo2/C toward Efficient Oxygen Reduction Reaction", Materials Today Energy, 18, (2020), 100557; Kottayintavida, R., Gopalan, N. K. "Pd Modified Ni Nanowire as an Efficient Electro-Catalyst for Alcohol Oxidation Reaction", International Journal of Hydrogen Energy, 45, (2020), 8396-8404.

[28]. Hanifah, M. F. R., Jaafar, J., Othman, M., Ismail, A., Rahman, M., Yusof, N., Aziz, F. "One-Pot Synthesis of Efficient Reduced Graphene Oxide Supported Binary Pt-Pd Alloy Nanoparticles as Superior Electro-Catalyst and Its Electro-Catalytic Performance toward Methanol Electro-Oxidation Reaction in Direct Methanol Fuel Cell", Journal of Alloys Compounds, 793, (2019), 232-246; Wang, J., Sun, H.-b., Shah, S. A., Liu, C., Zhang, G.-y., Li, Z., Zhang, Q.-f., Han, M. "Palladium Nanoparticles Supported by Three-Dimensional Freestanding Electrodes for High-Performance Methanol Electro-Oxidation", International Journal of Hydrogen Energy, 45, (2020), 11089-11096.

[29]. Li, Q., Bai, A., Xue, Z., Zheng, Y., Sun, H. "Nitrogen and Sulfur Co-Doped Graphene Composite Electrode with High Electrocatalytic Activity for Vanadium Redox Flow Battery Application", Electrochimica Acta, 362, (2020), 137223.